

Porosity and permeability evolution and evaluation in anisotropic porosity multiscale-multiphase-multicomponent structure

ZHU BoJing¹, CHENG HuiHong¹, QIAO YanChao¹, LIU Chang^{1,2}, SHI YaoLin^{1*}, ZHANG Kai³, SUN DongSheng⁴ & LIN WeiRen⁵

¹Key Laboratory of Computational Geodynamics, Chinese Academy of Sciences; College of Science, Graduate University of Chinese Academy of Sciences, Beijing 100049, China;

²Laboratoire De Geologie, Ecole Normale Supérieure, 24 Rue Lhomond, 75231 Paris CEDEX 5, France;

³Beijing Synchrotron Radiation Facility, Institute of High Energy Physics, Chinese Academy of Sciences, Beijing 100049, China;

⁴Geological Mechanics Institute, Chinese Academy of Geological Sciences, Beijing 100081, China;

⁵Kochi Institute for Core Sample Research, Japan Agency for Marine-Earth Science and Technology, Kochi 783-8502, Japan

Received July 12, 2011; accepted August 28, 2011

Based on the hybrid hypersingular integral equation-lattice Boltzmann methods (HHIE-LBM), the porosity and permeability evolution and evaluation process in anisotropic saturated porosity multiscale-multiphase-multicomponent (ASP-MS-MP-MC) structures under ultra high temperature and pressure conditions was analyzed on parallel CPU and GPU platforms. First, virtual physical models at multi-spatial scales (2 μm , 5 μm and 10 μm) were restructured by computerized microtomography technology and data. Second, using HHIE-LBM methods, the anisotropic porosity and permeability tensor at core level and pore level under ultra high temperature and pressure conditions were calculated. Third, the evolution and evaluation process of the porosity and permeability as a function of multi temporal spatial scales was investigated. Finally, the relationship between porosity and permeability and ASP-MS-MP-MC structures (micro-meso-macro-scale) was explored.

porosity and permeability tensor, anisotropic saturated porosity multiscale-multiphase-multicomponent structures, hypersingular integral equation method, lattice Boltzmann method, ultra temperature and pressure, parallel CPU and GPU

Citation: Zhu B J, Cheng H H, Qiao Y C, et al. Porosity and permeability evolution and evaluation in anisotropic porosity multiscale-multiphase-multicomponent structure. *Chin Sci Bull*, 2012, 57: 320–327, doi: 10.1007/s11434-011-4874-4

In the past 10 years, with developments in geophysics, seismology, mechanics and materials, the anisotropic saturated porosity multiscale-multiphase-multicomponent (ASP-MS-MP-MC) structures have attracted the attention of researchers for its wide application in these interdisciplinary fields. However, many micro-meso-macro mechanisms have not yet been clearly evaluated, especially with regard to their structural physical characteristics.

To investigate the porous physical character and structure problem, Berger [1] explored fabric tensors of anisotropic porous solids using boundary elements and the Green's function method. Roberts and Garboczi [2] studied elastic

properties of porous ceramics using a finite element method, and established the relationship between pore shape and structure. Almqvist et al. [3,4] used measured seismic velocities to analyze the elastic properties of anisotropic synthetic aggregates, containing mixtures of calcite and muscovite, under uniaxial loads ranging from 20 MPa up to 400 MPa. Zhang [5,6] presented the physical mechanism of fully and partially saturated geomaterials, and obtained significant results for the complex coupled fluid-solid system. Wei [7] provided the governing equation of static and dynamic behavior of multiphase porous media. Diabiraa et al. [8] discussed the porosity and permeability evolution accompanying hot fluid injection into the diatomite problem. Mark [9] explored permeability in fibrous porous media using the

*Corresponding author (email: shiy1@gucas.ac.cn)

LBM method. Lindquist et al. [10] explored permeability by studying pore and throat size distributions in X-ray tomography rock data. Zhu et al. [11] analyzed interfacial properties of pores and solids through microtomography rock data. Gu et al. [12] evaluated reservoir characteristics and genesis of high porosity and high permeability reservoirs in the Tarim basin. Jia and Gu [13] studied controlling factors and the porosity evolution process of high-quality sandstone reservoirs of the Kelas-2 gas field in the Kuqa depression. Zhao et al. [14] used experimental methods to study the three dimensional isotropic dielectric composite with negative permeability. Cong et al. [15] used experimental methods to study effects of porosity on acoustic resonance spectroscopy for synthetic highly porous rock samples. Based on the Sierpinski carpet and Menger sponge, Zhang et al. [16] developed new porosity models, which predict the cumulative porosity of rock and other samples. To investigate the micro scale level permeability problem, Yang et al. [17] discussed the permeability of MC-RR on the outer membranes of *Escherichia coli* and *Bacillus subtilis* (Bubtilis).

Nonetheless, few reports have used numerical methods to calculate the porosity and permeability evolution and evaluation under ultra high temperature and pressure conditions for ASP-MS-MP-MC structures. Studies also are lacking for complex constitutive relationships at different physical scales, coupled with thermal force fields and ultra large model data problems.

In this paper, we studied the porosity and permeability evolution and evaluation process of ASP-MS-MP-MC from a multidisciplinary perspective. First, based on previous works [18–20], and on computerized tomography technology, virtual physical models at different spatial scales (2 μm, 5 μm and 10 μm) were restructured on parallel CPU and GPU platforms. Second, the anisotropic porosity and permeability tensor at both core level and pore level under ultra high temperature and pressure conditions were calculated. Third, the evolution and evaluation process of porosity and permeability as a function of multi temporal spatial scales was investigated. Finally, the relationship between porosity and permeability and ASP-MS-MP-MC structure (micro-meso-macro-scale) was explored.

1 Basic equation

In the present paper, the summation from 1 to 3 over repeated lowercase, and of 1 to 6 in uppercase, for ASP-MS-MP-MC structures under electro-magneto-thermal-force (EMTF) coupled fields, may be expressed using extended differential governing equations, formulated as [21–28]

$$\left(C_{ijkl} e_{kl} - M_{ij} [\phi(U_i - u_i)] \right)_{ij,j} = \rho \ddot{u}_i + \rho_f \left(\frac{\partial [\phi(U_i - u_i)]}{\partial^2 t} \right)_i, \quad (1)$$

$$\left(M [\phi(U_i - u_i)] - M_{ij} e_{ij} \right)_i = \rho_f \ddot{u}_i + M_{ij} \left(\frac{\partial [\phi(U_j - u_j)]}{\partial^2 t} \right)_{,j} + r_{ij} \left(\frac{\partial [\phi(U_j - u_j)]}{\partial t} \right)_{,j}, \quad (2)$$

where

$$\begin{aligned} r_{ij} [\phi(U_j - u_j)]_{,j} &= \frac{\eta}{\text{Re} [K_{ij} \phi(U_j - u_j)]} M_{ij} [\phi(U_j - u_j)]_{,j} \\ &= \text{Re} [T_{ij} \phi(U_j - u_j)] / \phi, \\ T_{ij} [\phi(U_j - u_j)]_{,j} &= \bar{i} \eta \phi / K_{ij} [\phi(U_j - u_j)] \phi(U_j - u_j) \rho_f, \\ \rho &= (1 - \phi) \rho_s + \rho_f, \end{aligned}$$

where C_{ijkl} , e_{kl} , M_{ij} , ϕ , U_i , u_i , ρ , ρ_s , ρ_f , M , T_{ij} , K_{ij} indicate extended solid skeleton elastic modulus parameters, extended solid skeleton strain tensor, skeleton modulus parameters, extended porosity tensor, extended displacement of the solid skeleton, extended displacements of the pore fluid, bulk-fluid mixture density of skeleton-fluid system, density of the solid skeleton, density of the pore fluid, elastic modulus parameters of the pore fluid, dynamic tortuosity and dynamic permeability tensor, respectively.

If we consider turbulence of the fluid effects at the micro scale, the governing equations of fully saturated porous contracture can be formulated as [29]

$$\sigma_{ij,j}^e - \bar{\alpha} p_{,i} - [n \rho^w + (1 - n) \rho^s] \ddot{u}_i - n \rho^w (\ddot{u}_i^w - \ddot{u}_i^s) = 0, \quad (3)$$

$$-n p_{,i} - \rho^w \ddot{u}_i^w - n^2 \gamma^w k^{-1} (\dot{u}_i^w - \dot{u}_i^s) = 0, \quad (4)$$

$$\dot{p} [n(K^w)^{-1} + (\bar{\alpha} - n)(K^s)^{-1}] + (\bar{\alpha} - n) \dot{u}_{i,i}^s + n \dot{u}_{i,i}^w = 0, \quad (5)$$

where n , $\bar{\alpha}$, ρ^w , ρ^s , u_i^w , u_i^s , k , γ^w , K^w , K^s , p represent the porosity, the Boit parameter, the solid density, the fluid density, displacement of pore water, the displacement of solid skeleton, the permeability coefficient, the bulk density of pore water, the bulk modulus of pore water, the bulk modulus of solid grains and the pore water pressure, respectively. The basic strain equation for anisotropic saturated multiphase porous structures can be written as

$$\varepsilon_{ij} = \frac{1}{2G} \left[\sigma_{ij} - \frac{\nu}{1 + \nu} \delta_{ij} \sigma_{kk} + \frac{3(\nu_u - \nu)}{B(1 + \nu)(1 + \nu_u)} \delta_{ij} p \right], \quad (6)$$

$$m - m_0 = \left[\frac{3\rho_0(\nu_u - \nu)}{2GB(1 + \nu)(1 + \nu_u)} \right] \left(\sigma_{kk} + \frac{3p}{B} \right), \quad (7)$$

$$q_l = -\rho_0 k p_{,l}, \quad (8)$$

where σ_{ij} , ε_{ij} , m , G , ν , ν_u , m_0 , ρ_0 , q_l , B represent total stress, total strain and fluid mass per unit volume, elastic shear modulus, drained Poisson's ratio, undrained Poisson's ratio, fluid mass content in the unstressed state, mass density of

the pore fluid, mass flux rate per unit area, and the constant which relates to drained and undrained status, respectively. The extended pore stress can be formulated as

$$\sigma_p = P + \tau_{ij} = P - p\delta_{ij} + \bar{\sigma}_{ij}, \quad (9)$$

$$\bar{\sigma}_{ij} = \bar{\mu} \left(\bar{u}_{i,j}^w + \bar{u}_{j,i}^w - \frac{1}{3} \bar{u}_{l,l}^w \delta_{ij} \right) + \bar{\mu}' \bar{u}_{i,l}^w \delta_{ij} - \overline{\rho u_i^w u_j^w}, \quad (10)$$

$$\overline{\rho u_i^w u_j^w} = \bar{\mu}_t (u_{i,j}^{w'} + u_{j,i}^{w'}) - \frac{2}{3} (\rho E + \bar{\mu}_t u_{m,m}^{w'}), \quad (11)$$

where σ_p , P , τ_{ij} , p , $\bar{\sigma}_{ij}$, $\bar{\mu}$, $\bar{\mu}'$, \bar{u}_i^w , $u^{w'}$, E stand for extended pore stress, hydrostatic pressure, extended viscous shear force, internal hydrostatic pressure, extended viscous force, viscosity, isochoric viscosity, turbulent mean-velocity, turbulent fluctuation velocity and bulk modulus, respectively.

If we define surface porosity as the ratio of the area of voids in a plane cross section of the ASP-MS-MP-MC structures with respect to total area of the cross section, then the second-order surface porosity tensor can be written as [30]

$$\phi_{ij} = v_j w_i^{-1}, \quad (12)$$

where v_j and w_i represent the average true velocity and the seepage velocity, respectively.

The permeability tensor of the ASP-MS-MP-MC structures can be written as

$$K_{ij} = \phi_{ik} \phi_{kj}, \quad (13)$$

where ϕ_{kj} is the hydraulic form factor tensor [30].

2 Porosity and permeability

2.1 HHIE-LBM model

Based on previous work [1], it is known that the HHIE method is useful in studies of skeleton solid crack initiation, and propagation and transmission problems at multi temporal spatial scales (yellow color in Figure 1 indicates the

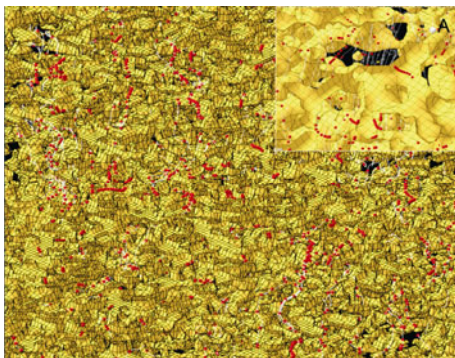


Figure 1 Flow driven pore-network crack model at multi spatial scales.

core solid skeleton part of the material); whereas the LBM method may be used to successfully evaluate flow driven fluid pore problems at multi temporal spatial scales (black color in Figure 1 represents flow pores).

By combining the two methods, we may then study the coupled pore and core interface extended stress of micro-meso-macro-scale ASP-MS-MC structures by establishing the relationship between extended pore fluid pressure and extended core stress. This method also allows us to analyze porosity and permeability under different initial and boundary conditions. A more detailed introduction can be found elsewhere in the literature [31–33].

Based on the D3Q27 HHIE-LBM model [18], the virtual ASP-MS-MP-MC model can be established. As shown in Figure 2, green spheres indicate the solid skeleton (core) and yellow spheres signify pore fluid (pore). Each fluid sphere can be described by a D3Q27 model, and the distance between two spheres is defined as the resolution of the physical model. Then, the multi spatial scale model may be explored by using three different resolution values.

Figure 3 shows the original physical rock model, where the diameter of the sample is equal to 25 mm and the length of the sample is equal to 30 mm. The top cross section of the physical model is defined as the x - y plane, and the length is represented by the z coordinate direction (from top to bottom). Using technology, the differential spatial scale

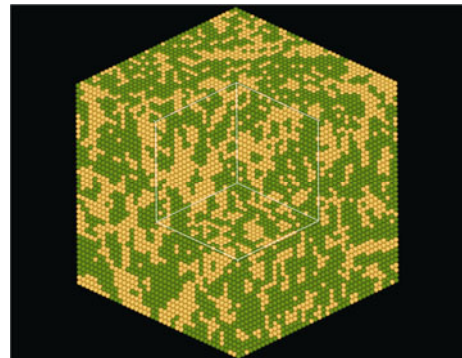


Figure 2 HHIE-LBM model for porosity and permeability tensor.

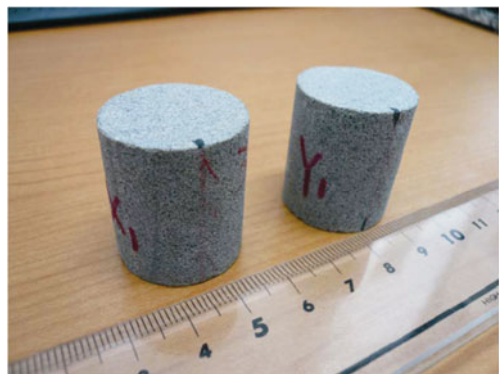


Figure 3 Granite physical model (diameter=25 mm, length=30 mm).

virtual physical model can be restructured.

Using JAMSTEC (Japanese Agency for Marine Earth Science and Technology) X-CT data, the anisotropic 10 μm/pix slice resolution virtual HHIE-LBM model was established (Figures 4 and 5).

Based on BSRF (Beijing Synchrotron Radiation Facility) micro-CT (4W1A light, magnetic density=1.8 T) data, a similar anisotropic 5 μm/pix slice resolution and 2 μm/pix slice resolution virtual HHIE-LBM can be established (Figures 6 and 7).

The top-right portion of Figure 6 represents a random part of the virtual physical model at the scale I level. With increasing resolution, the width of the image decreases. The main part of Figure 6 shows the microstructure one-eighth of the top-right at scale II level.

The bottom-right section of Figure 7 represents a random portion of the virtual physical model at the scale II level, and the main part in Figure 7 shows the microstructure of a

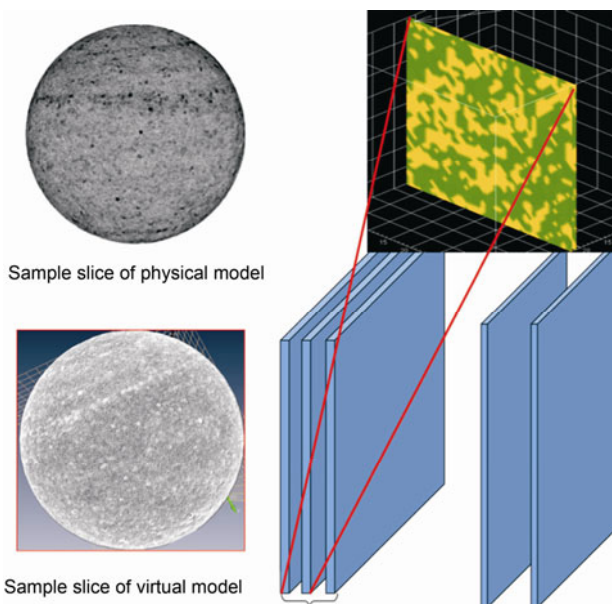


Figure 4 Restructure progress of physical-virtual HHIE-LBM model.

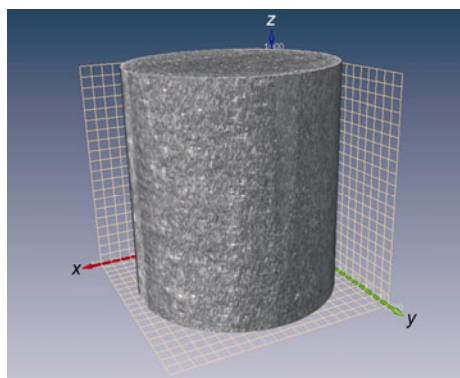


Figure 5 HHIE-LBM model at scale I (10 μm resolution).

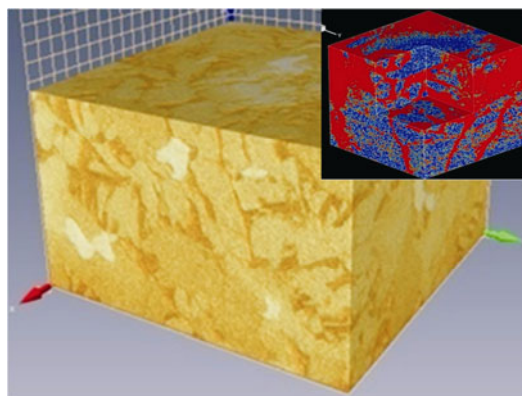


Figure 6 HHIE-LBM model at scale II (5 μm resolution).

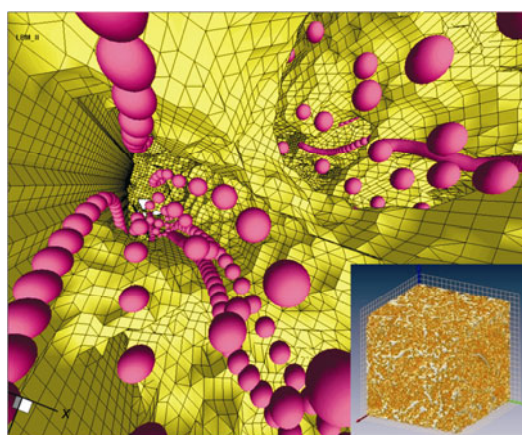


Figure 7 HHIE-LBM model at scale I (2 μm resolution).

random portion in the bottom-right part of the material at the scale III level.

From Figures 6 and 7, we also can see that at scale III level, the anisotropic porosity and permeability character of the multiscale-multiphase-multicomponent can be analyzed using numerical methods. Then, utilizing statistical mechanics theory, the macro anisotropic porosity and permeability tensor of the virtual physical multiscale-multiphase-multicomponent at differential spatial scales can be defined and calculated.

2.2 Porosity and permeability tensor under ultra high temperature and pressure

To simulate ASP-MS-MP-MC porosity and permeability under the ultra high temperature and pressure condition, we adopted a temperature of 300°C and pressure of 1000 MPa pressure. The formulation of the appearance porosity tensor and micro permeability tensor are written as [8,34]

$$\Phi_{ij} = \begin{bmatrix} \Phi_{11} & \Phi_{12} & \Phi_{13} \\ \Phi_{21} & \Phi_{22} & \Phi_{23} \\ \Phi_{31} & \Phi_{32} & \Phi_{33} \end{bmatrix}, \quad (14)$$

$$\kappa_{ij} = \begin{bmatrix} \kappa_{11} & \kappa_{12} & \kappa_{13} \\ \kappa_{21} & \kappa_{22} & \kappa_{23} \\ \kappa_{31} & \kappa_{32} & \kappa_{33} \end{bmatrix}. \quad (15)$$

Then, the appearance porosity tensor can be calculated using the HHIE-LBM method.

Figures 8–10 show porosity as a function of spatial position at different scales. From Figure 8, we can see that only the *z* direction anisotropic character is clear. When the resolution was equal to 5 μm (Figure 9), the anisotropic character clearly was in the three principal axes direction. In addition, when the resolution reached 2 μm (Figure 10), the simulation reflected anisotropy in all directions. This level provided the most reasonable model. Therefore, in this paper, the 2 μm resolution model was used to analyze porosity and permeability as a function of temporal and spatial scales at ultra high temperature and pressure.

Figure 10 shows the components of the apparent porosity tensor as a function of spatial position (three principle axes directions and three shear axes directions), and Figures 11–13 show the micro permeability tensor as a function of *x*, *y* and *z*, respectively. The arrow vector stands for the component vectors of porosity and the contour represents permeability density.

2.3 Evolution and evaluation process of porosity and permeability as a function of multi temporal spatial scales

Figure 14 shows the micro permeability evolution and evaluation process of ASP-MS-MP-MC structure as a function of time. With increasing time, the interface between the pore and core part appears twisted, deformed and fused. At the same time, multi-crystal defects, dislocation and crack initiation and propagation took place. These characteristics

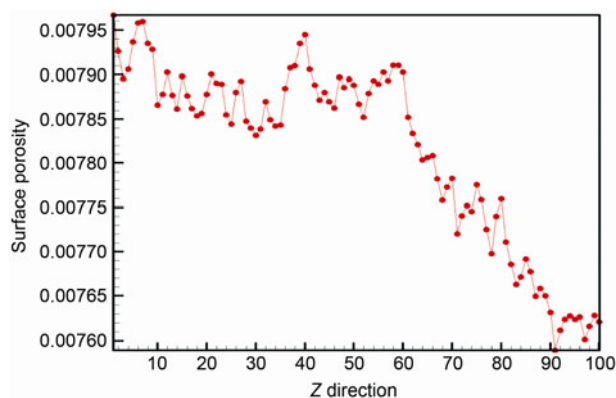


Figure 8 Porosity tensor of ASP-MS-MP-MC structure at 300°C, 1000 MPa and 10 μm resolution.

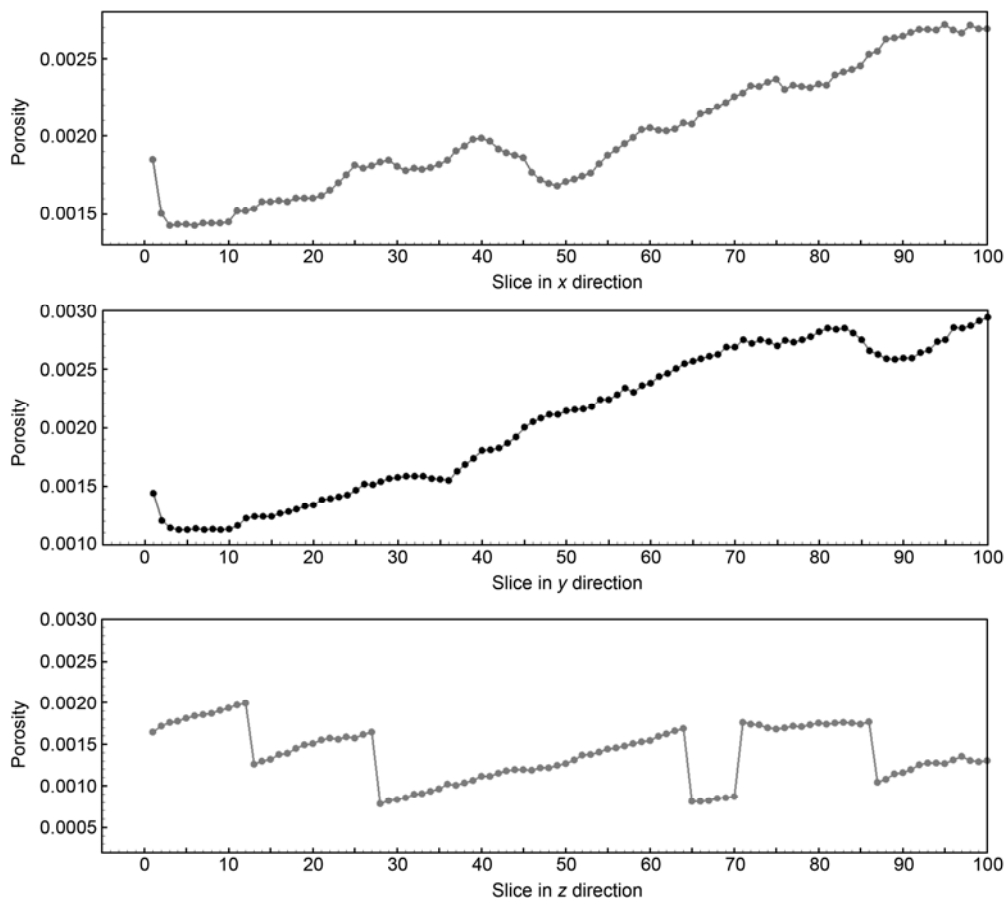


Figure 9 Porosity tensor of ASP-MS-MP-MC structure at 300°C, 1000 MPa and 5 μm resolution.

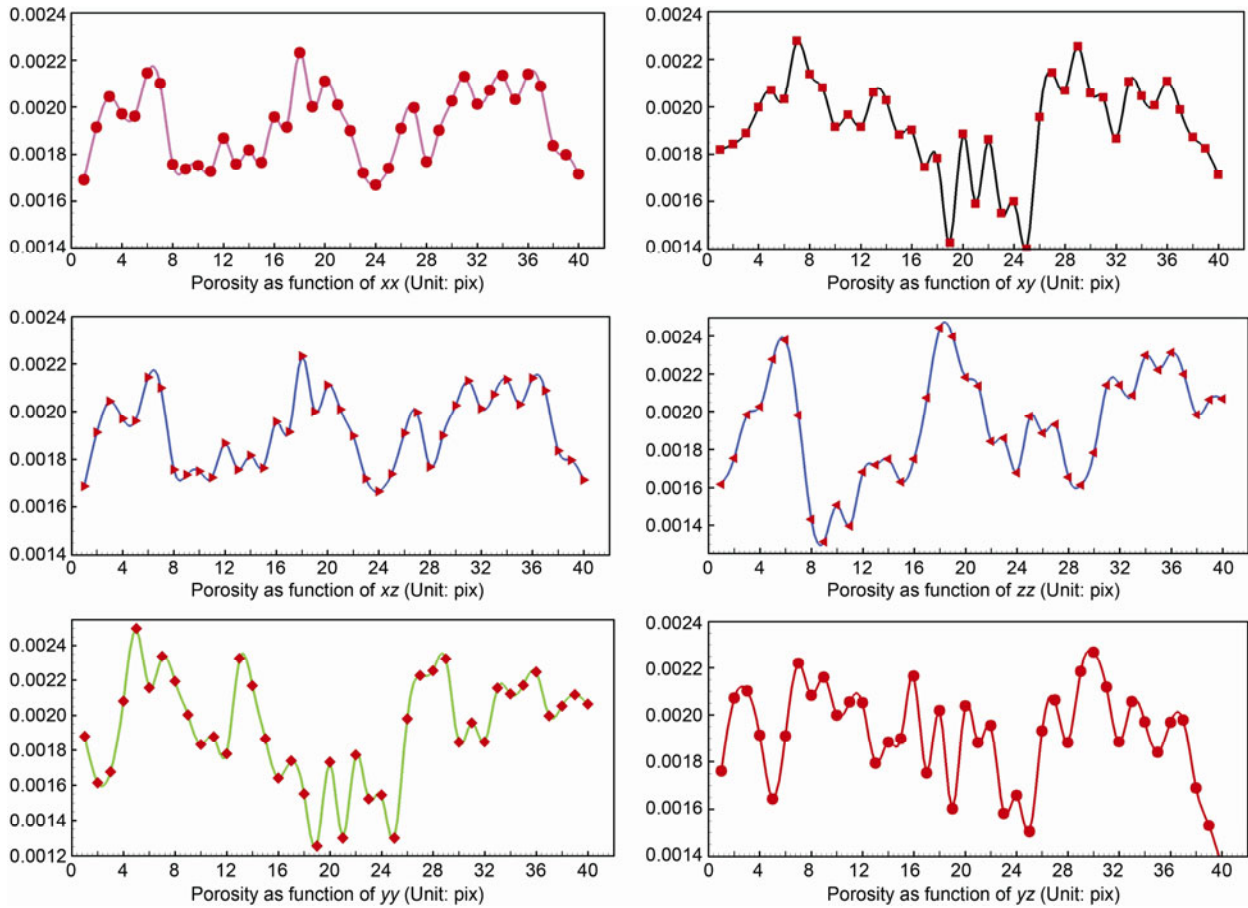


Figure 10 Porosity tensor of ASP-MS-MP-MC structure at 300°C and 1000 MPa.

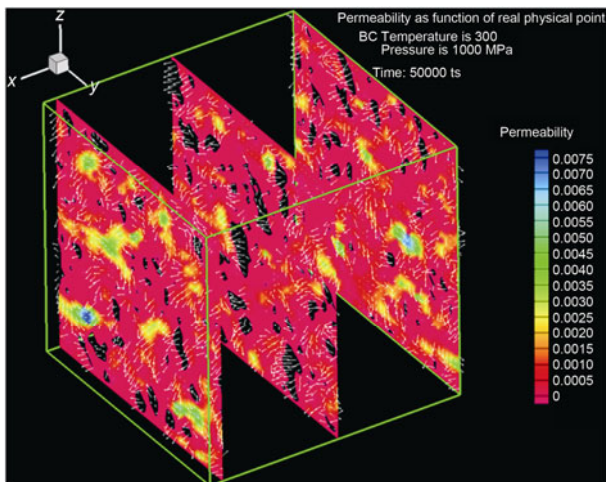


Figure 11 Permeability tensor of ASP-MS-MP-MC structure as a function of x under a temperature of 300°C and pressure of 1000 MPa.

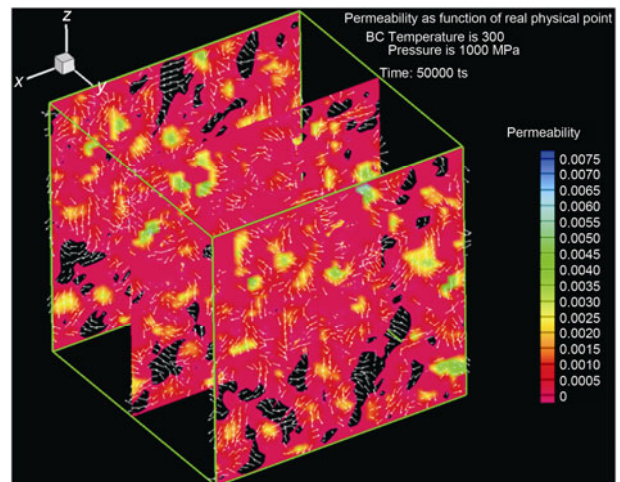


Figure 12 Permeability tensor of ASP-MS-MP-MC structure as a function of y under temperature of 300°C and pressure of 1000 MPa.

caused the structure of ASP-MS-MP-MC to change, and the strength of the material at macro performance level decreased. A more detailed exploration of the coupled fluid-solid interface at the lowest scale level will provide more evidence for the relationship between micro structure and macro performance for ASP-MS-MP-MC structures.

3 Discussion and conclusions

Based on the hybrid hypersingular integral equation-lattice Boltzmann method proposed herein, the porosity and permeability evolution and evaluation process in anisotropic saturated porosity multiscale-multiphase-multicomponent structure

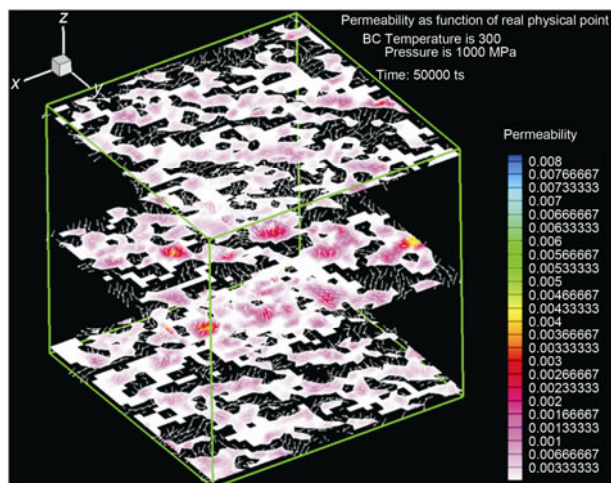


Figure 13 Permeability tensor of ASP-MS-MP-MC structure as a function of z under a temperature of 300°C and pressure of 1000 MPa.

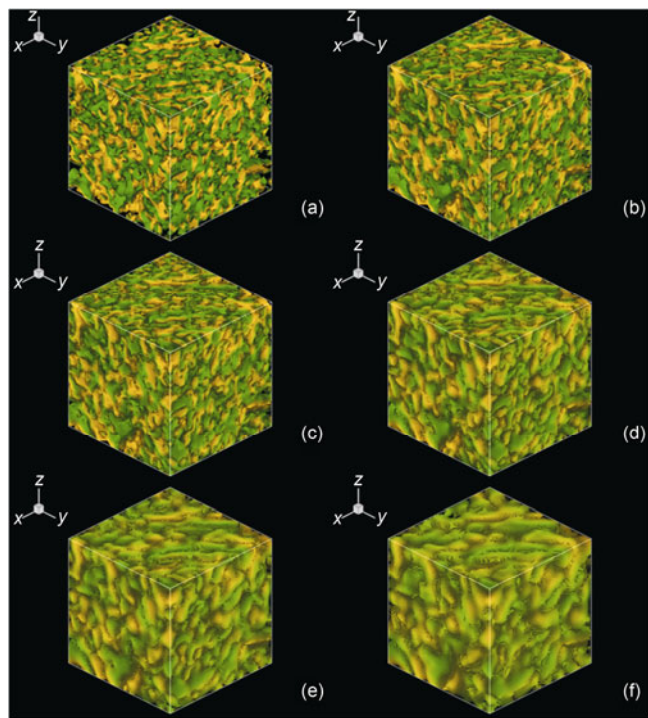


Figure 14 Permeability evolution and evaluation process of ASP-MS-MP-MC structure as a function of time under temperature of 300°C and pressure of 1000 MPa.

under ultra high temperature and pressure conditions was analyzed at parallel CPU and GPU platforms for the first time. The results are summarized as follows:

(1) The virtual physical model at different spatial scales was restructured, and the anisotropic porosity and permeability tensor at core level and pore level at a temperature of 300°C and pressure of 1000 MPa was investigated;

(2) The evolution and evaluation process of porosity and permeability as a function of multi temporal spatial scales, and the relationship between porosity and permeability and

ASP-MS-MP-MC structure were explored.

These results will assist in a better understanding of the mechanisms between microstructure and macro-performance, and can be applied to the fields of geophysics and seismology.

We thank Professor Teng-Fong Wong and Professor David A. Yune for helpful discussions and comments on this paper. This work was supported by the Project SinoProbe-07 of China, the National Natural Science Foundation of China (D0408/4097409), the First Class Foundation of Graduate University of the Chinese Academy of Sciences (Y15101KY00), the Knowledge Innovation Program of the Chinese Academy of Sciences (KJCX2-YW-N42) and the Key Important Project of the National Natural Science Foundation of China (10734070).

- Berger J R. Fabric tensor based boundary element analysis of porous solids. *Eng Anal Bound Elem*, 2011, 35: 430–435
- Roberts A P, Garboczi E J. Elastic properties of model porous ceramics. *J Am Ceram Soc*, 2000, 83: 3041–3048
- Almqvist B G. Physical anisotropies in deformed carbonate rocks. Dissertation for Master Degree. Ontario, Canada: Lakehead University, 2010
- Almqvist B G, Burlini L, Mainprice D, et al. Elastic properties of anisotropic synthetic calcite-muscovite aggregates. *J Geophys Res*, 2010, 115: 1–15
- Zhang H W, Schrefler B A. Particular aspects of internal length scales in strain localization analysis of multiphase porous materials. *Comput Methods Appl Mech Eng*, 2004, 193: 2867–2884
- Zhang H W. Strain Localisation Analysis for Fully and Partially Saturated Geomaterials. Hannover: Universitat Hannover Press, 2001
- Wei C. Static and dynamic behavior of multiphase porous media: Governing equations and finite element implementation. Dissertation for Doctoral Degree. Norman, OK: The University of Oklahoma, 2001
- Diabiraa I, Castaniera L M, Kovscek A R. Porosity and permeability evolution accompanying hot fluid injection into diatomite. *Petrol Sci Tech*, 2001, 19: 1167–1185
- Mark A, Doormaal V, Pharoah J G. Determination of permeability in fibrous porous media using the lattice Boltzmann method with application to PEM fuel cells. *Int J Numer Meth Fluids*, 2009, 59: 75–89
- Lindquist W B, Venkatarangan A, Dunsmuir J, et al. Pore and throat size distributions measured from synchrotron X-ray tomographic images of frontainebleau sandstones. *J Geophys Res*, 2000, 105: 21509–21527
- Zhu W L, Glenn A G, Fusses F, et al. Microtomography of partially molten rocks: Three-dimensional melt distribution in mantle peridotite. *Science*, 2011, 332: 88–91
- Gu J Y, Jia J H, Fang H. Reservoir characteristics and genesis of high-porosity and high-permeability reservoirs in Tarim Basin. *Chin Sci Bull*, 2002, 47: 12–19
- Jia J H, Gu J Y. Control factors and porosity evolution of high-quality sandstone reservoirs of Kela-2 gas field in Kuqa Depression. *Chin Sci Bull*, 2002, 47: 100–106
- Zhao Q, Kang L, Zhao H J, et al. Isotropic negative permeability composite based on Mie resonance of the BST-MgO dielectric medium. *Chin Sci Bull*, 2008, 53: 3272–3276
- Cong J S, Wang X M, Xu D L, et al. Experimental studies on the effects of porosity on acoustic resonance spectroscopy for synthetic porous rock samples in acylindrical resonant cavity. *Chin Sci Bull*, 2008, 53: 978–983
- Zhang J R, Tao G L, Huang L, et al. Porosity models for determining the pore-size distribution of rocks and soils and their applications. *Chin Sci Bull*, 2010, 55: 3960–3970
- Yang C Y, Xia C H, Zhou S W, et al. The permeability effect of microcystin-RR on *Escherichia coli* and *Bacillus subtilis*. *Chin Sci Bull*, 2010, 55: 1894–1898
- Zhu B J, Shi Y L. Three-dimensional flow driven pore-crack networks in porous composites: Boltzmann Lattice method and hybrid hypersingular integrals. *Theor Appl Fract Mech*, 2010, 53: 9–41

- 19 Zhu B J, Shi Y L, Sukop M C, et al. Analysis of 3D fluid driven crack propagation problem in co-seismic slip under P- and S-waves by hybrid hypersingular integral method. *Comput Meth Appl Mech Eng*, 2009, 198: 2446–2469
- 20 Zhu B J, Liu C, Shi Y L, et al. Application of flow driven pore-network crack model to Zipingpu reservoir and Longmenshan slip. *Sci China Phys Mech Astron*, 2011, 54: 1532–1540
- 21 Liu Y, Gao L T. Energy focusing and the shapes of wave fronts in anisotropic fluid-saturated porous media. *Acta Mech*, 2007, 193: 207–225
- 22 Sharma M D. Wave propagation in a general anisotropic poroelastic medium with anisotropic permeability: Phase velocity and attenuation. *Int J Solids Struc*, 2004, 41: 4587–4597
- 23 Sharma M D. Wave propagation in anisotropic generalized thermoelastic media. *J Therm Stresses*, 2006, 29: 629–642
- 24 Biot M A. General theory of three-dimensional consolidation. *J Appl Phys*, 1941, 12: 155–164
- 25 Biot M A. Theory of elasticity and consolidation for a porous anisotropic solid. *J Appl Phys*, 1955, 26: 182–187
- 26 Biot M A. Theory of propagation of elastic waves in a fluid-saturated porous solid. 1. Low-frequency range. *J Acoust Soc Am*, 1956, 28: 168–178
- 27 Biot M A. Theory of propagation of elastic waves in a fluid-saturated porous solid. 2. Higher frequency range. *J Acoust Soc Am*, 1956, 28: 179–191
- 28 Zhu B J, Qin T Y. Application of hypersingular integral equation method to three-dimensional crack in electromagnetoelastomeric multiphase composites. *Int J Solids Struc*, 2007, 44: 5994–6012
- 29 Lewis R W, Schrefler B A. *The Finite Element Method in the Static and Dynamic Deformation and Consolidation of Porous Media*. 2nd ed. Chichester: Wiley and Sons, 1999
- 30 Dmitriev N M. Surface porosity and permeability of porous media with a periodic microstructure. *Fluid Dyn*, 1995, 30: 64–69
- 31 Qin T Y, Tang R J. Finite-part integral and boundary-element method to solve embedded planar crack problems. *Int J Fracture*, 1993, 60: 373–381
- 32 Kuo C Y, Frost J D, Chameau J L. Image analysis determination of stereology based fabric tensors. *Geotechnique*, 1998, 48: 515–525
- 33 Koo J M, Kleinstreuer C. Liquid flow in microchannels: Experimental observations and computational analyses of microfluidics effects. *J Micromech Microeng*, 2003, 13: 568–579
- 34 Holmes M H, Mow V C. The nonlinear characteristics of soft cells and hydrated connective tissues in ultrafiltration. *J Biomech*, 1990, 23: 1145–1156

Open Access This article is distributed under the terms of the Creative Commons Attribution License which permits any use, distribution, and reproduction in any medium, provided the original author(s) and source are credited.